Journal of Non-Crystalline Solids 419 (2015) 58–64

Contents lists available at ScienceDirect

Journal of Non-Crystalline Solids

journal homepage: www.elsevier.com/ locate/ jnoncrysol

Fracture toughness of calcium–silicate–hydrate from molecular dynamics simulations

M. Bauchy [a,*], H. Laubie [b], M.J. Abdolhosseini Qomi [b], C.G. Hoover [b], F.-J. Ulm [b,c], R.J.-M. Pellenq [b,c,d]

[a] Physics of AmoRphous and Inorganic Solids Laboratory (PARISlab), Department of Civil and Environmental Engineering, University of California, Los Angeles, CA 90095, United States
[b] Concrete Sustainability Hub, Department of Civil and Environmental Engineering, Massachusetts Institute of Technology, 77 Massachusetts Avenue, Cambridge, MA 02139, United States
[c] MIT-CNRS Joint Laboratory at Massachusetts Institute of Technology, 77 Massachusetts Avenue, Cambridge, MA 02139, United States
[d] Centre Interdisciplinaire des Nanosciences de Marseille, CNRS and Aix-Marseille University, Campus de Luminy, Marseille, 13288 Cedex 09, France

ARTICLE INFO

Article history:
Received 12 March 2015
Received in revised form 26 March 2015
Accepted 28 March 2015
Available online xxxx

Keywords:
Calcium–silicate–hydrate;
Fracture toughness;
Surface energy;
Molecular dynamics

ABSTRACT

Concrete is the most widely manufactured material in the world. Its binding phase, calcium–silicate–hydrate (C–S–H), is responsible for its mechanical properties and has an atomic structure fairly similar to that of usual calcium silicate glasses, which makes it appealing to study this material with tools and theories traditionally used for non-crystalline solids. Here, following this idea, we use molecular dynamics simulations to evaluate the fracture toughness of C–S–H, inaccessible experimentally. This allows us to discuss the brittleness of the material at the atomic scale. We show that, at this scale, C–S–H breaks in a ductile way, which prevents one from using methods based on linear elastic fracture mechanics. Knowledge of the fracture properties of C–S–H at the atomic scale opens the way for an upscaling approach to the design of tougher cement paste, which would allow for the design of slender environment-friendly infrastructures, requiring less material.

1. Introduction

Concrete is the most used material in the world after water [1]. Thanks to its low cost, cement is the only material that can satisfy the growing demand for infrastructure, especially in developing countries. However, the production of cement is responsible for about 7% of the global emissions of carbon dioxide in the atmosphere [2]. Because of such a ubiquitous presence in our environment, only a small decrease in its production would have a significant impact in terms of greenhouse gas emissions. To this end, one option is to improve the toughness of the cementitious matrix in concrete. Indeed, a tougher cement paste would allow using less material while achieving comparable mechanical properties. Moreover, an increased resistance to fracture would improve its longevity, making it more sustainable.

Calcium–silicate–hydrate (C–S–H), the binding phase of the cement paste, can be seen as a gel [3], made of grains with a poor degree of crystallinity, if any [4]. Due to its multi-scale [5] and heterogeneous [6] nature, the fracture mechanism of C–S–H remains largely unknown. In particular, the intrinsic fracture toughness of C–S–H grains at the atomic scale remains unknown, and it would be challenging to obtain it experimentally. This knowledge would serve as a basis to build a multi-scale model of fracture in C–S–H, following a bottom-up approach. Despite the prevalence of concrete in the built environment, the molecular structure of C–S–H has just recently been proposed [7–10,4], which makes it possible to investigate its mechanical properties at the atomic scale.

Hence, relying on this newly available model, we computed the fracture toughness and critical energy release rate of C–S–H at the atomic scale by means of molecular dynamics simulations. On the other hand, the computation of its surface energy allowed us to quantify its brittleness. This paper is organized as follows. We first present the details of the simulation of C–S–H in Section 2 and discuss its glassy nature. The methodology used to obtain the fracture toughness is detailed in Section 3. Results are reported in Section 4 and discussed in Section 5. Some conclusions are finally presented in Section 6.

2. Simulation details

2.1. C–S–H model

To describe the disordered molecular structure of C–S–H, Pellenq et al. [7] proposed a realistic model for C–S–H with the stoichiometry of $(CaO)_{1.65}(SiO_2)(H_2O)_{1.73}$. We generated the C–S–H model by introducing defects in an 11 Å tobermorite [11] configuration, following a combinatorial procedure. Whereas the Ca/Si ratio in 11 Å tobermorite is 1, this ratio is increased to 1.71 in the present C–S–H model, through randomly introducing defects in the silicate chains, which provides sites for adsorption of extra water molecules. The REAXFF potential [8], a reactive potential, was then used to account for the reaction of the interlayer water with the defective calcium–silicate sheets. More details on

* Corresponding author.
E-mail address: bauchy@ucla.edu (M. Bauchy).
URL: http://mathieu.bauchy.com (M. Bauchy).

http://dx.doi.org/10.1016/j.jnoncrysol.2015.03.031
0022-3093/

the preparation of the model and its experimental validation can be found in Ref. [9] and in previous works [4,7,10,12–16].

We simulated the previously presented C–S–H model, made of 501 atoms, by molecular dynamics using the LAMMPS package [18]. To this end, we used the REAXFF potential [8] with a time step of 0.25 fs. We first relaxed the system at zero pressure and 300 K during 2.5 ns in the NPT and NVT ensembles and made sure that convergence of the energy and volume was achieved.

2.2. C–S–H as an amorphous material

To validate the structure of the model, we computed the X-ray pair distribution function (PDF):

$$g_X(r) = \frac{1}{\sum_{i,j=1}^{n} c_i c_j b_i b_j} \sum_{i,j=1}^{n} c_i c_j b_i b_j g_{ij}(r) \quad (1)$$

where b_i is the X-ray scattering length for i atoms, which we assumed to be constant as in Ref. [17]. Note that, to take into account the maximum scattering vector Q_{max} of the experimental structure factor, the computed PDFs were broadened by following the methodology described in Refs. [19,20].

Fig. 1 shows the X-ray PDF of C–S–H, compared with experimental data obtained by Monteiro et al. [21,22,17] for a synthetic C–S–H specimen with Ca/Si = 1.6, fairly similar to the present composition. The first peak, around 1.0 Å, arises from H–O correlations. H–H correlations inside water molecules are merged with the peak around 1.6 Å, which corresponds to Si–O correlations around Si tetrahedra. The signification of the following peaks is less clear as they arise from a superposition of several correlations; however Ca–O, O–O, and Si–Si correlations are, respectively, observed around 2.3, 2.7, and 3.2 Å. We note a good agreement between simulation and experiment for C–S–H, which is remarkable considering the complexity of the material. In particular, the positions and heights of the first peaks, associated with Si–O, Ca–O and Si–Si correlations, respectively, are well reproduced by the simulation. Although the general shape at high r is also well reproduced, we observe a slight shift of the Si–Ca peak. Overall, the atomic structure appears to be similar to that of a silicate glass [23], with the PDF showing broad peaks. However, although the system is globally disordered, a direct observation of the atomic configuration (see Fig. 2) reveals that it maintains the layered structure characteristic of the tobermorite crystal [11,10,14,4].

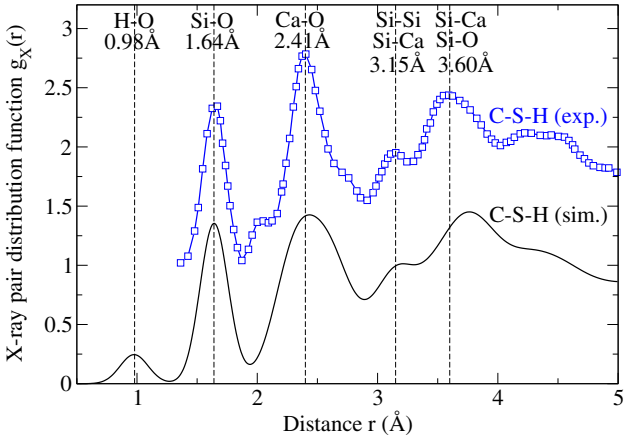

Fig. 1. X-ray pair distribution function of the calcium–silicate–hydrate model, compared with experimental data for a synthetic C–S–H with Ca/Si = 1.6 [17].

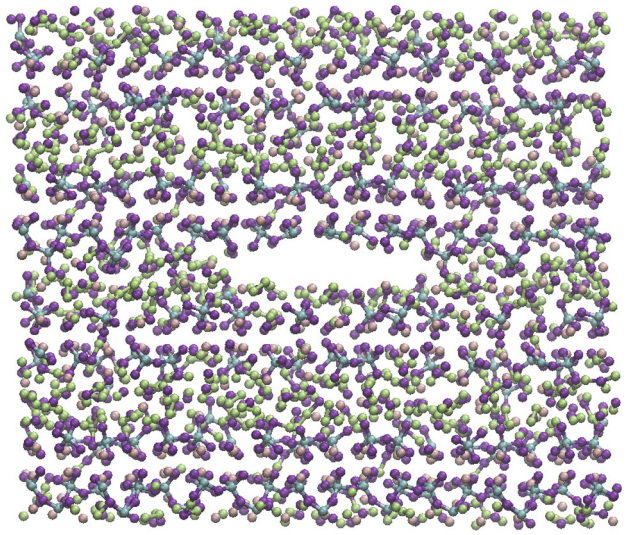

Fig. 2. Snapshot of the atomic configuration of the calcium–silicate–hydrate model, with an initial crack. Silicon, oxygen, calcium, and hydrogen atoms are respectively represented in cyan, purple, pink, and green.

3. Fracture toughness computation

3.1. Computation of the fracture energy

To study the propagation of an initial crack in the material, the initial cell was replicated in x, y and z directions. The smallest considered system was made of $1 \times 2 \times 2$ initial cells, whereas the biggest one was built by a $2 \times 5 \times 3$ replication. Fig. 2 shows a snapshot of the atomic configuration of a $1 \times 3 \times 2$ C–S–H model. After the replication, each system was relaxed during 1 ns in NPT and NVT ensembles.

Traditional methods of determining fracture energy, for example using the classic path independent J-integral evaluation either analytically [24,25] or numerically [26], will not work for this investigation because they assume a large specimen made of a continuous homogeneous material, such that the stresses emanating from and surrounding the crack tip are uninfluenced by structural boundaries. Other models such as the so-called *Work of Fracture* method or *fictitious crack model* of Hillerborg [27] and enshrined in a RILEM international recommendation [28], which relates the external work to the internal energy release rate (similar proposals were made for ceramics [29,30]), are also not applicable for the same reasons. Other methods such as utilizing the linear elastic fracture mechanics (LEFM) energy release rate functions for known geometries [31] or approximations for more complicated geometries using the Jenq–Shah model [32,33], which can also yield crack extension, are not applicable for this type of analysis. Therefore, another method must be adopted.

Recently, Brochard et al. [34] introduced a new method to study fracture properties at the smallest scales, based on molecular dynamics simulations. This approach relies on the energetic theory of fracture mechanics [35–37] and consists of thermodynamic integration during crack propagation. This method does not involve any assumption about the mechanical behavior of the material during the fracture and can thus capture fracture properties of brittle as well as ductile systems [34]. Note that it has been successfully used to compute the fracture toughness of silicate glasses [38,39].

In the following, we focus on fracture in mode I, i.e., with an opening mode and a loading normal to the crack plane. A crack is first initiated into a molecular sample. We restrict ourselves to the propagation of cracks in planes parallel to the calcium layers, that is, the direction of fracture along the z axis being the weakest, as it does not involve any bond breaking inside the silicate chains. We also focus on crack propagation inside interlayer spaces, where both structural and free water

can be found, as it is the weakest point of rupture in the system. Such cracks are expected to exist naturally in real materials and allow us to control in which interlayer space the crack will propagate. The initial crack is created by removing atoms located inside an elliptic volume along the x direction. The ellipse is chosen to be five times larger in the y direction than in the z direction, thus inducing a strong concentration of the stress at the crack tips. Its length goes from 12 to 50 Å, depending on the size of the supercell. Note that the initial length must be long enough for the initial hole to be stable but small as compared with the box length in the y direction.

Before any tension is applied, the system is fully relaxed to be unstressed; thus, its mechanical energy P, involved by strain, becomes zero. The procedure then consists in increasing the size L_z of the system in the direction orthogonal to the initial crack until its full propagation along the y axis. L_z is incremented stepwise by 1% of its initial unstressed value L_{z0} up to $L_{z\max} = 1.5L_{z0}$. After each increase of the tensile strain $\epsilon = (L_z - L_{z0})/L_{z0}$, the system is relaxed for 5 ps before performing a statistical averaging stage for another 5 ps. During the latter phase, the stress in the z direction σ_z is computed with the virial equation [40].

Note that the entire fracture simulation is operated within the canonical NVT ensemble, in which the temperature is controlled by a Nose–Hoover thermostat [41,42]. Hence, we are unable to capture potential heat transfers during the fracture. In fact, this procedure has not been designed to model the kinetics of crack propagation. On the contrary, thermodynamic quantities are always integrated when the system is at equilibrium, at each strain step. The phonons that arise during the fracture are annealed by the thermostat, as it will be shown later (see Section 4). Therefore, phonons are not included in the following thermodynamic integration.

As the crack starts to propagate, some elastic energy P is released to create new surface. This is captured by the energy release rate G:

$$G = -\frac{\partial P}{\partial A} \tag{2}$$

where A is the crack area. When propagation occurs, the energy release rate is equal to the critical energy release rate G_c, which is considered as a property of the material. Once the crack propagation is complete, the system becomes unstressed again, so that $P = 0$, the mechanical energy having been released by crack propagation. The integration of σ_z over the whole process, i.e., the external work, thus provides the critical energy release rate G_c:

$$G_c = \frac{\Delta F}{\Delta A} = \frac{L_x L_y}{\Delta A_\infty}\int_{L_{z0}}^{L_{z\max}} \sigma_z dL_z \tag{3}$$

where F is the free energy of the system and $\Delta A_\infty = A_\infty - A_0$ is the total area of surface created at the end of the fracture, when the crack has fully propagated. This formula is a direct consequence of Griffith theory of fracture [35]. It is worth noting that evaluating the crack area at the end of the fracture may not be straightforward as the created surface may show some roughness. To make an accurate estimate of the critical energy release rate, the real surface area has been calculated using the procedure proposed in Ref. [34].

3.2. Fracture toughness calculation

Alternatively to the energetic approach, the notion of fracture toughness K_{Ic} is usually used in engineering application. This quantity was introduced by Irwin [43] as the maximum stress intensity at the crack tip a solid can undergo, and below which propagation cannot occur. The relationship between K_{Ic} and G_c is given by the Irwin formula [43]:

$$G_c = H_I K_{Ic}^2 \tag{4}$$

where H_I is given in Ref. [44] for transversely isotropic solids and can be written in terms of the stiffness constants C_{ij}, using Voigt notation, as:

$$H_I = \frac{1}{2}\sqrt{\frac{C_{11}}{C_{11}C_{33} - C_{13}^2}\left(\frac{1}{C_{44}} + \frac{2}{C_{13} + \sqrt{C_{11}C_{33}}}\right)} \tag{5}$$

in plane strain, as is the case of the current study. Note that, although we rely on a general energetic approach that does not assume a purely brittle fracture, we keep in mind that the relation between G_c and K_{Ic} was derived in the context of LEFM. The full elastic tensor C_{ij} was computed for a bulk system, before the introduction of the initial crack. The elements of the stiffness tensor are obtained by calculating the curvature of the potential energy U with respect to small strain deformations ϵ_i [45]:

$$C_{ij} = \frac{1}{V}\frac{\partial^2 U}{\partial \epsilon_i \partial \epsilon_j} \tag{6}$$

where V is the volume of the system. In isotropic materials, Eq. (4) reduces to the usual Irwin formula [36]:

$$G_c = \frac{1-\nu^2}{E}K_{Ic}^2 \tag{7}$$

where E is the Young's modulus. However, C–S–H is not an isotropic material, as the Young's modulus in the direction perpendicular to the calcium layers is lower than that in the plane of the layers [9].

3.3. Validation with glassy silica

Before being applied to C–S–H, the present methodology was tested on a usual silica glass, prepared by using the BKS potential [46–48]. Fig. 3 shows the computed stress σ_z with respect to the tensile strain ϵ. At low strain, up to 12%, the mechanical response is fairly linear elastic. The stress increases linearly with the strain, up to around 9 GPa, with the slope related to the Young's modulus of the system. During this stage, the crack does not propagate and the free energy of the system is stored in the form of mechanical elastic energy only. At larger strain, the crack starts to propagate. As shown in Fig. 3, silica shows a typical brittle fracture, as the crack suddenly propagates above a critical strain of 13%. This manifests by a drop of the tensile stress to zero, which is comparable to what has been observed for quartz [34].

After integration of the stress–strain curve of glassy silica, we find $G_c = 9.2\ \mathrm{J/m^2}$ and $K_{Ic} = 0.81\ \mathrm{MPa\cdot m^{1/2}}$, which is in excellent agreement with available experimental data ($G_c = 9.0 \pm 0.4\ \mathrm{J/m^2}$ and $K_{Ic} = 0.81 \pm 0.02\ \mathrm{MPa\cdot m^{1/2}}$ [49]). Hence, we feel confident to apply the present

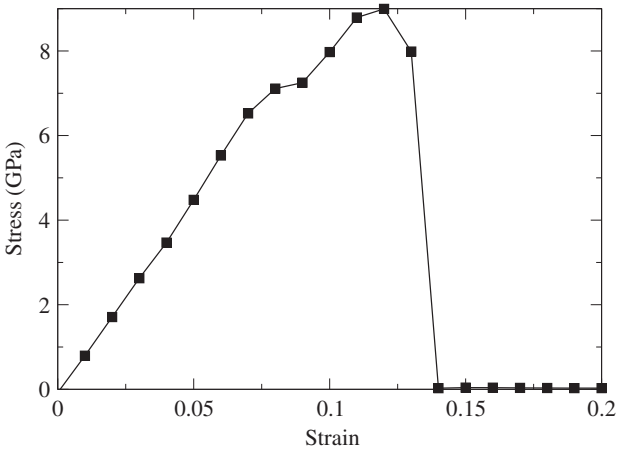

Fig. 3. Computed stress as a function of the tensile strain imposed to a silica glass.

model to C–S–H. More details regarding the use of the present methodology for silicate glasses can be found in Refs. [38,39].

4. Results

Fig. 4 shows the computed stress σ_z with respect to the tensile strain ϵ for a C–S–H sample. The simulated system is 13.1 Å × 54.4 Å × 46.8 Å in volume, with an initial crack of 15 Å. Similarly to silica, at low strain, the mechanical response is linear elastic and, at larger strain, the crack starts to propagate. However, the maximum stress appears to be lower than in the case of glassy silica (only 1.4 GPa, as opposed to 9 GPa for silica) and is achieved at lower strain (0.06, as opposed to 0.12). This significant difference arises from the fact that C–S–H features some weak layers, filled by calcium ions and water molecules. This decreases the stiffness and strength of C–S–H with respect to a fully polymerized material like glassy silica.

In addition, as opposed to brittle materials like glassy silica or quartz [34], C–S–H shows a strong ductile behavior in the sense that the crack does not propagate instantly after a given critical strain. Thanks to its internal flexibility, the network rather deforms to prevent the fracture from occurring, as it observed in the snapshots inside Fig. 4. At large strain (from 20%), only one molecular chain made of calcium and oxygen atoms still exists between the up and down phases. The latter eventually breaks as soon as the strain reaches 26%.

The ductile behavior that is observed requires an extra care: indeed, as the crack propagates, irreversible processes, such as plasticity, occur inside a process zone around the crack tip. An estimated length of this plasticity zone r_{pl} can be evaluated using the Dugdale–Barenblatt formula [50–52]:

$$r_{pl} = \frac{\pi}{8}\left(\frac{K_{Ic}}{\sigma_{pl}}\right)^2 \tag{8}$$

where σ_{pl} is the plastic yield stress of the material. In the present C–S–H sample, we find $r_{pl} = 13.7$ Å, which is significantly larger than the value found in quartz (3.4 Å [34]) but remains lower to what can be found in kerogen (19.9 Å [34]). At the end of the fracture, the process zones located at both sides of the crack eventually overlap because of the periodic boundary conditions. As suggested in Ref. [34], this feature can be taken into account by replacing in Eq. (3) the real crack area ΔA_∞ by an effective area given by $\Delta A_{\infty,eff} = \Delta A_\infty - L_x r_{pl}/2$.

To get an estimation of the precision of the computed fracture toughness, five additional fracture simulations with different box and initial crack lengths were run. Even if each stress–strain curve is specific to each considered system, the resulting fracture toughness values remain consistent. This allows us to evaluate the standard deviations of the fracture properties as being $G_c = 1.72 \pm 0.29$ J/m^2 and $K_{Ic} = 0.369 \pm 0.030$ MPa·m$^{1/2}$. Thee values are significantly lower than the ones obtained for glassy silica, which is consistent with the fact that water molecules depolymerize the silicate chains in C–S–H.

Although, to the best of our knowledge, no experimental value of the fracture toughness of C–S–H at the scale of the grain is presently available, this value can be compared with available measurements in cement paste. Depending on the method used, the water-to-cement ratio and the age of the paste, the fracture toughness of cement paste is usually found between 0.29 and 0.40 MPa·m$^{1/2}$ [53–57]. However, despite this apparent agreement, we keep in mind that the cement paste is a complex inhomogeneous phase containing C–S–H particles, ettringite crystals, calcium hydroxide, monosulfoaluminates, and pores of different sizes, which obviously prevents a direct comparison.

Although our values, obtained at the atomic scale, cannot be directly compared with experimental results, obtained at much larger scales, the fact that the values are of the same order supports the ability of the present simulations to provide realistic results.

A posteriori, we check that there is no contribution to the fracture energy of the phonons in the equilibrated system after fracture. To this end, we compute the vibrational density of state (VDOS) $g(\omega)$ before and after the full propagation of the crack. This is achieved by calculating the Fourier-transform of the velocity autocorrelation function (VAF) [23]:

$$g(\omega) = \sum_{j=1}^{N} m_j \int_{-\infty}^{\infty} \mathrm{VAF}_j(t) exp(i\omega t) dt \tag{9}$$

where $\mathrm{VAF}_j(t)$ is the VAF of the atomic species j:

$$\mathrm{VAF}_j(t) = \frac{1}{Nk_BT} < \mathbf{v}_j(t)\mathbf{v}_j(0) > \tag{10}$$

and where N is the number of atoms, m_j is the mass of an atom j, ω is the frequency, and $\mathbf{v}_j(t)$ is the velocity of an atom j. Fig. 5 shows the VDOS of C–S–H, both before and after fracture. Unfortunately, no experimental VDOS is currently available for C–S–H. However, we note that it is very similar to that typically observed in silicate glasses [23], but features additional peaks at high frequency due to the H–O bonds. As expected, the VDOS does not change significantly after the fracture has happened. This is not surprising since, as mentioned before, the system is always at equilibrium with a thermostat during the fracture process in the present methodology.

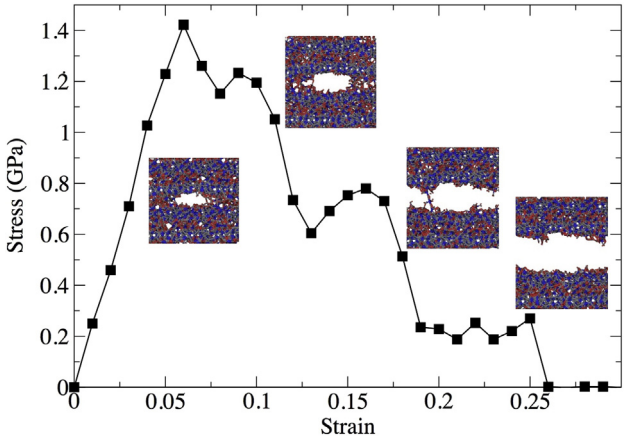

Fig. 4. Computed stress as a function of the tensile strain imposed to the system. The snapshots show the molecular configurations at different stages of the fracture.

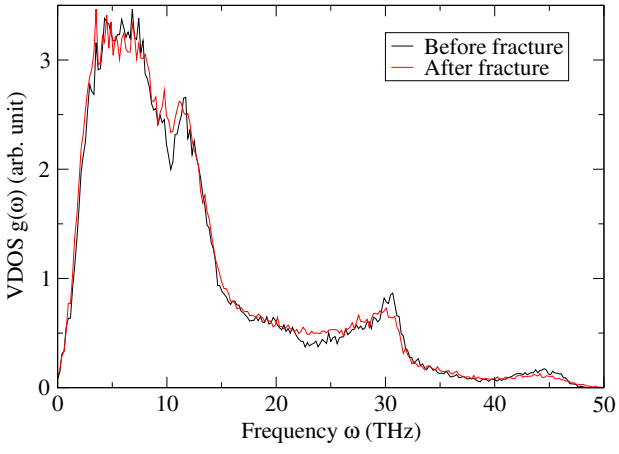

Fig. 5. Vibrational density of state (VDOS) of C–S–H at 300 K, both before (black curve) and after (red curve) the full propagation of the crack in the box.

5. Discussion

We now aim to quantify the brittleness of C–S–H at the atomic scale. The critical energy release rate G_c can be expressed from the surface energy γ_s:

$$G_c = 2\gamma_s + G_{\text{diss}} \tag{11}$$

where G_{diss} captures all forms of dissipated energy linked to irreversible processes and is equal to zero for a perfectly brittle material. The surface energy γ_s was roughly estimated from molecular dynamics simulation by cutting the system into two parts, letting it relax for 25 ps, and computing the change of the potential energy of the system. For the present C–S–H sample, we find $2\gamma_s = 1.06$ J/m^2. This value is fairly comparable to the surface energy of tobermorite gel, which is $2\gamma_s = 0.8$ J/m^2 [58]. Note that we observe the dissociation of some free water molecules during the fracture. As, e.g., Si–O–Ca bonds break, terminal 1-fold O and under-coordinated Ca atoms are energetically unfavorable: therefore, the following chemical reaction occurs:

$$(-\text{Si–O–Ca–}) + \text{H}_2\text{O} \rightarrow (-\text{Si–O–H}) + (\text{H–O–Ca–}) \tag{12}$$

This reaction obviously stabilizes the newly created surface, thus decreasing the surface energy. This stabilization can be observed in Fig. 6 as it manifests by a gradual decrease of the potential energy after the fracture. This highlights that, to study the fracture of such a hydrated material by molecular dynamics, it is critical to use a reactive potential that can handle such chemical reactions. The use of a classic non-reactive potential would result in an overestimation of the fracture energy.

The knowledge of the surface energy allows estimating $G_{\text{diss}} = 0.66$ J/m^2, as well as a lower bound of the fracture toughness $K_{Ic,\text{min}}$, i.e., the value one would get if no energy were dissipated during the fracture process. We find that $K_{Ic,\text{min}} = 0.289$ MPa·m$^{1/2}$. The analysis allows quantifying the ductility of the material by computing a brittleness parameter $B = 2\gamma_s/G_c$, which is equal to 1 for a perfectly brittle material. Here, we find $B = 0.62$, which highlights the fact that the fracture of C–S–H at the atomic scale involves ductility and, therefore, cannot be captured by methods that only rely on the theory of fracture in brittle materials. The energy dissipated during the fracture can arise from different phenomena, such as plasticity or crack blunting. This will be investigated in future works.

Through all these findings, the question remains if a ductile response is to be expected on larger scales. All the specimens simulated in this study have a plastic zone length extending approximately 14 Å from the crack tip. The plastic zone, in the continuum sense, is a nonlinear zone where characterized by progressive softening [59]. If the plastic zone size is very small compared to all relative dimensions of the simulation, then it can be approximated as a point, in which the models developed in LEFM can apply. However, if the plastic zone is non-negligible compared to specimen sizes, the specimens undergo progressive softening damage (due to mechanisms such as collective rearrangement of atoms or bond breakages) and stable crack propagation, where, for every increment in crack length, a stable equilibrium is obtained [59]. Here, the plastic zone that is found approaches the size of the C–S–H particles (around 3–5 nm [60]). This suggests that C–S–H should break in a ductile way at the nanoscale. Note that this is not in contradiction with the observed macroscale brittleness, as fracture behaviors depend on the considered scale [61]. Such nano-ductility has for example been shown to exist in typical macro-brittle materials like glasses [62,38]. The types of materials that have a fixed plastic zone length and exhibit a ductile behavior for small specimen sizes and a brittle behavior for large sizes are known as quasibrittle because their behavior is size dependent [61]. Methods exist which can extract fracture properties from such material behaviors [63–66]. Further investigation on bulk C–S–H is needed to determine if the brittleness of the specimen increases with system size.

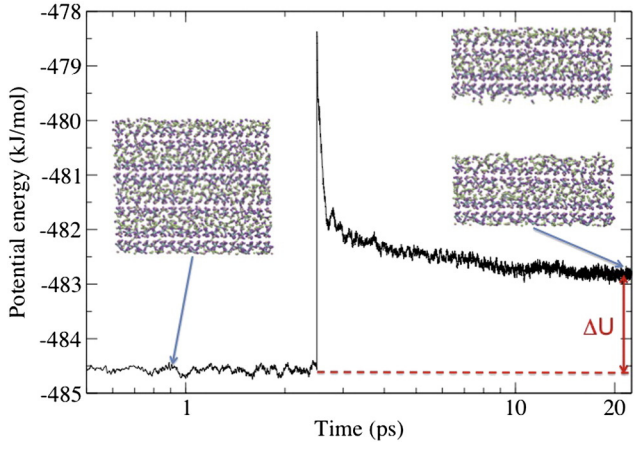

Fig. 6. Potential energy of C–S–H as a function of time. At $t = 2.5$ ps, the system is cut into two parts.

6. Conclusion

By using a realistic model of C–S–H as well as a molecular dynamics-based method allowing the capture of non-elastic effects, we computed the values of the surface energy, fracture toughness, and critical energy release rate of C–S–H grains, which are not directly accessible from experiments. At the atomic-scale, C–S–H appears to break in a ductile way, so that one cannot rely on LEFM-based methods. The intrinsic fracture toughness of C–S–H grains appears to be very close to that of the cement paste obtained by different experimental techniques. This suggests that the C–S–H grains play a major role in the fracture of cement.

It is now necessary to upscale this result to the meso- and, eventually, the macro-scales to enable direct comparisons with experiments as well as the design of a tougher material using a bottom-up approach. As a preliminary step, starting from the atomistic scale, one should study how the use of additives to C–S–H can result in tougher concrete. This could be achieved by tuning the elastic modulus and/or by maximizing the ductility to dissipate more energy during the fracture.

Acknowledgments

MB acknowledges partial financial support for this research provisioned by the University of California, Los Angeles (UCLA). This work was also supported by Schlumberger under an MIT-Schlumberger research collaboration and by the CSHub at MIT. This work has been partially carried out within the framework of the ICoME2 Labex (ANR-11-LABX-0053) and the A*MIDEX projects (ANR-11-IDEX-0001-02) cofunded by the French program "Investissements d'Avenir" which is managed by the ANR, the French National Research Agency.

References

[1] K. Scrivener, P. Wray, Straight talk with Karen Scrivener on cements, CO_2 and sustainable development, Am. Ceram. Soc. Bull. 91 (2012) 47–50 (URL https://infoscience.epfl.ch/record/178423).
[2] P.K. Mehta, Reducing the environmental impact of concrete, Concr. Int. 23 (10) (2001) 61–66 (URL http://ecosmartconcrete.com/docs/trmehta01.pdf).
[3] H.M. Jennings, Colloid model of C–S–H and implications to the problem of creep and shrinkage, Mater. Struct. 37 (1) (2004) 59–70, http://dx.doi.org/10.1007/BF02481627 (URL http://link.springer.com/article/10.1007/BF02481627).
[4] M. Bauchy, M.J. Abdolhosseini Qomi, F.-J. Ulm, R.J.-M. Pellenq, Order and disorder in calcium–silicate–hydrate, J. Chem. Phys. 140 (21) (2014) 214503, http://dx.doi.org/10.1063/1.4878656 (URL http://scitation.aip.org/content/aip/journal/jcp/140/21/10.1063/1.4878656).
[5] E. Masoero, E. Del Gado, R.J.-M. Pellenq, F.-J. Ulm, S. Yip, Nanostructure and nanomechanics of cement: polydisperse colloidal packing, Phys. Rev. Lett. 109 (15) (2012) 155503, http://dx.doi.org/10.1103/PhysRevLett.109.155503 (URL http://link.aps.org/doi/10.1103/PhysRevLett.109.155503).

[6] A.J. Allen, J.J. Thomas, H.M. Jennings, Composition and density of nanoscale calcium–silicate–hydrate in cement, Nat. Mater. 6 (4) (2007) 311–316, http://dx.doi.org/10.1038/nmat1871 (URL http://www.nature.com/nmat/journal/v6/n4/abs/nmat1871.html).

[7] R.J.-M. Pellenq, A. Kushima, R. Shahsavari, K.J.V. Vliet, M.J. Buehler, S. Yip, F.-J. Ulm, A realistic molecular model of cement hydrates, Proc. Natl. Acad. Sci. 106 (38) (2009) 16102–16107, http://dx.doi.org/10.1073/pnas.0902180106 (URL http://www.pnas.org/content/106/38/16102).

[8] H. Manzano, S. Moeini, F. Marinelli, A.C.T. van Duin, F.-J. Ulm, R.J.-M. Pellenq, Confined water dissociation in microporous defective silicates: mechanism, dipole distribution, and impact on substrate properties, J. Am. Chem. Soc. 134 (4) (2012) 2208–2215, http://dx.doi.org/10.1021/ja209152n (URL http://dx.doi.org/10.1021/ja209152).

[9] M.J. Abdolhosseini Qomi, K.J. Krakowiak, M. Bauchy, K.L. Stewart, R. Shahsavari, D. Jagannathan, D.B. Brommer, A. Baronnet, M.J. Buehler, S. Yip, F.-J. Ulm, K.J. Van Vliet, R.J.-M. Pellenq, Combinatorial molecular optimization of cement hydrates, Nature Communications 5 (2014) http://dx.doi.org/10.1038/ncomms5960. URL http://www.nature.com/ncomms/2014/140924/ncomms5960/full/ncomms5960.html.

[10] J. Abdolhosseini Qomi, M. Bauchy, R.J.-M. Pellenq, F.-J. Ulm, Applying tools from glass science to study calcium–silicate–hydrates, Mechanics and Physics of Creep, Shrinkage, and Durability of Concrete: A Tribute to Zdenek P. Bazant, Proceedings of the Ninth International Conference on Creep, Shrinkage, and Durability Mechanics (CONCREEP-9), September 22–25, 2013 Cambridge, MassachusettsASCE Publications 2013, pp. 78–85, http://dx.doi.org/10.1061/9780784413111.008.

[11] S. Hamid, The crystal-structure of the 11-a natural tobermorite Ca2.25[si3o7.5(oh)1.5].1h2o, Z. Kristallogr. 154 (3–4) (1981) 189–198, http://dx.doi.org/10.1524/zkri.1981.154.3-4.189.

[12] M.J. Abdolhosseini Qomi, M. Bauchy, F.-J. Ulm, R.J.-M. Pellenq, Anomalous composition-dependent dynamics of nanoconfined water in the interlayer of disordered calcium–silicates, J. Chem. Phys. 140 (5) (2014) 054515, http://dx.doi.org/10.1063/1.4864118 (URL http://scitation.aip.org/content/aip/journal/jcp/140/5/10.1063/1.4864118).

[13] M. Bauchy, M.J. Abdolhosseini Qomi, C. Bichara, F.-J. Ulm, R.J.-M. Pellenq, Nanoscale structure of cement: viewpoint of rigidity theory, J. Phys. Chem. C 118 (23) (2014) 12485–12493, http://dx.doi.org/10.1021/jp502550z (URL http://dx.doi.org/10.1021/jp502550z).

[14] M. Bauchy, M.J. Abdolhosseini Qomi, R.J.M. Pellenq, F.J. Ulm, Is cement a glassy material? Comput. Model. Concr. Struct. 169 (2014).

[15] M. Bauchy, M.J.A. Qomi, C. Bichara, F.-J. Ulm, R.J.-M. Pellenq, Topological origin of fracture toughening in complex solids: the viewpoint of rigidity theory, 2014. arXiv:1410.2916 [cond-mat]ArXiv: 1410.2916. URL http://arxiv.org/abs/1410.2916.

[16] M. Bauchy, M.J.A. Qomi, C. Bichara, F.-J. Ulm, R.J.-M. Pellenq, Rigidity transition in materials: hardness is driven by weak atomic constraints, Phys. Rev. Lett. 114 (12) (2015) 125502, http://dx.doi.org/10.1103/PhysRevLett.114.125502 (URL http://link.aps.org/doi/10.1103/PhysRevLett.114.125502).

[17] S. Soyer-Uzun, S.R. Chae, C.J. Benmore, H.-R. Wenk, P.J.M. Monteiro, Compositional evolution of calcium silicate hydrate (C–S–H) structures by total X-ray scattering, J. Am. Ceram. Soc. 95 (2) (2012) 793–798, http://dx.doi.org/10.1111/j.1551-2916.2011.04989.x (URL http://onlinelibrary.wiley.com/doi/10.1111/j.1551-2916.2011.04989.x/abstract).

[18] S. Plimpton, Fast parallel algorithms for short-range molecular dynamics, J. Comput. Phys. 117 (1) (1995) 1–19 (URL http://cat.inist.fr/?aModele=afficheN&cpsidt=11066050).

[19] M. Bauchy, Structural, vibrational, and elastic properties of a calcium aluminosilicate glass from molecular dynamics simulations: the role of the potential, J. Chem. Phys. 141 (2) (2014) 024507, http://dx.doi.org/10.1063/1.4886421 (URL http://scitation.aip.org/content/aip/journal/jcp/141/2/10.1063/1.4886421).

[20] A.C. Wright, The comparison of molecular dynamics simulations with diffraction experiments, J. Non-Cryst. Solids 159 (3) (1993) 264–268, http://dx.doi.org/10.1016/0022-3093(93)90232-M (URL http://www.sciencedirect.com/science/article/pii/002230939390232M).

[21] L.B. Skinner, S.R. Chae, C.J. Benmore, H.R. Wenk, P.J.M. Monteiro, Nanostructure of calcium silicate hydrates in cements, Phys. Rev. Lett. 104 (19) (2010) 195502, http://dx.doi.org/10.1103/PhysRevLett.104.195502 (URL http://link.aps.org/doi/10.1103/PhysRevLett.104.195502).

[22] C. Meral, C.J. Benmore, P.J.M. Monteiro, The study of disorder and nanocrystallinity in C–S–H, supplementary cementitious materials and geopolymers using pair distribution function analysis, Cem. Concr. Res. 41 (7) (2011) 696–710, http://dx.doi.org/10.1016/j.cemconres.2011.03.027 (URL http://www.sciencedirect.com/science/article/pii/S0008884611001037).

[23] M. Bauchy, Structural, vibrational, and thermal properties of densified silicates: Insights from molecular dynamics, J. Chem. Phys. 137 (4) (2012) 044510, http://dx.doi.org/10.1063/1.4738501 (URL http://scitation.aip.org/content/aip/journal/jcp/137/4/10.1063/1.4738501).

[24] J.R. Rice, Mathematical analysis in the mechanics of fracture, Fract. Adv. Treatise 2 (1968) 191–311.

[25] J.R. Rice, A path independent integral and the approximate analysis of strain concentration by notches and cracks, J. Appl. Mech. 35 (2) (1968) 379–386.

[26] V. Šmilauer, C.G. Hoover, Z.P. Bažant, F.C. Caner, A.M. Waas, K.W. Shahwan, Multiscale simulation of fracture of braided composites via repetitive unit cells, Eng. Fract. Mech. 78 (6) (2011) 901–918, http://dx.doi.org/10.1016/j.engfracmech.2010.10.013 (URL http://www.sciencedirect.com/science/article/pii/S0013794410004625).

[27] A. Hillerborg, The theoretical basis of a method to determine the fracture energy G F of concrete, Mater. Struct. 18 (4) (1985) 291–296, http://dx.doi.org/10.1007/BF02472919 (URL http://link.springer.com/article/10.1007/BF02472919).

[28] Rilem, Determination of the fracture energy of mortar and concrete by means of three-point bend tests on notched beams, Mater. Struct. 18 (4) (1985) 287–290, http://dx.doi.org/10.1007/BF02472918 (URL http://dx.doi.org/10.1007/BF02472918).

[29] J. Nakayama, Direct measurement of fracture energies of brittle heterogeneous materials, J. Am. Ceram. Soc. 48 (11) (1965) 583–587, http://dx.doi.org/10.1111/j.1151-2916.1965.tb14677.x (URL http://onlinelibrary.wiley.com/doi/10.1111/j.1151-2916.1965.tb14677.x/abstract).

[30] H.G. Tattersall, G. Tappin, The work of fracture and its measurement in metals, ceramics and other materials, J. Mater. Sci. 1 (3) (1966) 296–301, http://dx.doi.org/10.1007/BF00550177 (URL http://link.springer.com/article/10.1007/BF00550177).

[31] H. Tada, P.C. Paris, G.R. Irwin, The Analysis of Cracks Handbook, ASME Press, New York, 2000.

[32] Y.S. Jenq, S.P. Shah, A Fracture toughness criterion for concrete, Eng. Fract. Mech. 21 (5) (1985) 1055–1069, http://dx.doi.org/10.1016/0013-7944(85)90009-8 (URL http://www.sciencedirect.com/science/article/pii/0013794485900098).

[33] Y. Jenq, S. Shah, Two parameter fracture model for concrete, J. Eng. Mech. 111 (10) (1985) 1227–1241, http://dx.doi.org/10.1061/(ASCE)0733-9399(1985)111:10(1227) (URL http://ascelibrary.org/doi/abs/10.1061/).

[34] L. Brochard, G. Hantal, H. Laubie, F. Ulm, R. Pellenq, Fracture mechanisms in organic-rich shales: role of Kerogen, Poromechanics V, vol. 5, American Society of Civil Engineers 2013, pp. 2471–2480.

[35] A.A. Griffith, The phenomena of rupture and flow in solids, philosophical transactions of the royal society of London, Philos. Trans. R. Soc. Lond. Ser. A 221 (1921) 163–198.

[36] J.-B. Leblond, Mecanique de la rupture fragile et ductile, lavoisier edition Lavoisier, Paris, 2003.

[37] T.L. Anderson, Fracture Mechanics: Fundamentals and Applications, CRC Press LLC, 2005.

[38] B. Wang, Y. Yu, Y.J. Lee, M. Bauchy, Intrinsic nano-ductility of glasses: the critical role of composition, Glass Sci. 2 (2015) 11, http://dx.doi.org/10.3389/fmats.2015.00011 (URL http://journal.frontiersin.org/Journal/10.3389/fmats.2015.00011/abstract).

[39] Y. Yu, B. Wang, Y.J. Lee, M. Bauchy, Fracture toughness of silicate glasses: insights from molecular dynamics simulations, Symposium UU — Structure–Property Relations in Amorphous Solids, MRS Online Proceedings Library, vol. 1757, 2015http://dx.doi.org/10.1557/opl.2015.50 (URL http://journals.cambridge.org/article_S1946427415000500).

[40] M.P. Allen, D.J. Tildesley, Computer Simulation of Liquids, Oxford Science Publications, Clarendon Press, Oxford, 1987.

[41] S. Nosé, A molecular dynamics method for simulations in the canonical ensemble, Mol. Phys. 52 (2) (1984) 255–268, http://dx.doi.org/10.1080/00268978400101201 (URL http://www.tandfonline.com/doi/abs/10.1080/00268978400101201).

[42] W.G. Hoover, Canonical dynamics: equilibrium phase-space distributions, Phys. Rev. A 31 (3) (1985) 1695–1697, http://dx.doi.org/10.1103/PhysRevA.31.1695 (URL http://link.aps.org/doi/10.1103/PhysRevA.31.1695).

[43] G.R. Irwin, Fracture in "Handbuch der Physik", vol. V, Springer, New York, NY, 1958.

[44] G.C. Sih, P. Paris, G. Irwin, On cracks in rectilinearly anisotropic bodies, Int. J. Fract. Mech. 1 (3) (1965) 189–203.

[45] A. Pedone, G. Malavasi, A.N. Cormack, U. Segre, M.C. Menziani, Insight into elastic properties of binary alkali silicate glasses; prediction and interpretation through atomistic simulation techniques, Chem. Mater. 19 (13) (2007) 3144–3154, http://dx.doi.org/10.1021/cm062619r.

[46] K. Vollmayr, W. Kob, K. Binder, Cooling-rate effects in amorphous silica: a computer-simulation study, Phys. Rev. B 54 (22) (1996) 15808–15827, http://dx.doi.org/10.1103/PhysRevB.54.15808 (URL http://link.aps.org/doi/10.1103/PhysRevB.54.15808).

[47] A. Roder, W. Kob, K. Binder, Structure and dynamics of amorphous silica surfaces, J. Chem. Phys. 114 (17) (2001) 7602–7614, http://dx.doi.org/10.1063/1.1360257 (URL http://scitation.aip.org/content/aip/journal/jcp/114/17/10.1063/1.1360257).

[48] F. Yuan, L. Huang, Brittle to ductile transition in densified silica glass, Sci. Rep. 4 (2014) http://dx.doi.org/10.1038/srep05035. (URL http://www.nature.com/srep/2014/140522/srep05035/full/srep05035.html.

[49] S.M. Wiederhorn, Fracture surface energy of glass, J. Am. Ceram. Soc. 52 (2) (1969) 99–105, http://dx.doi.org/10.1111/j.1151-2916.1969.tb13350.x (URL http://onlinelibrary.wiley.com/doi/10.1111/j.1151-2916.1969.tb13350.x/abstract).

[50] D. Dugdale, Yielding of steel sheets containing slits, J. Mech. Phys. Solids 8 (2) (1960) 100–104.

[51] G. Barenblatt, The mathematical theory of equilibrium cracks in brittle fracture, Adv. Appl. Mech. 7 (55–129) (1962) 104.

[52] J.M. Lemm, Advances in Applied Mechanics, Academic Press, 1962.

[53] V.S. Dwivedi, P.L. Pratt, Strength, fracture and deformation behaviour of Portland cement paste, ICF6, New Delhi (India) 1984, 2013.

[54] J.S. Nadeau, S. Mindess, J.M. Hay, Slow crack growth in cement paste, J. Am. Ceram. Soc. 57 (2) (1974) 51–54, http://dx.doi.org/10.1111/j.1151-2916.1974.tb10811.x (URL http://onlinelibrary.wiley.com/doi/10.1111/j.1151-2916.1974.tb10811.x/abstract).

[55] D.D. Higgins, J.E. Bailey, Fracture measurements on cement paste, J. Mater. Sci. 11 (11) (1976) 1995–2003, http://dx.doi.org/10.1007/BF02403347 (URL http://link.springer.com/article/10.1007/BF02403347).

[56] B. Hillemeier, H.K. Hilsdorf, Fracture mechanics studies on concrete compounds, Cem. Concr. Res. 7 (5) (1977) 523–535, http://dx.doi.org/10.1016/0008-8846(77)90114-4 (URL http://www.sciencedirect.com/science/article/pii/0008884677901144).

[57] J.H. Brown, C.D. Pomeroy, Fracture toughness of cement paste and mortars, Cem. Concr. Res. 3 (4) (1973) 475–480, http://dx.doi.org/10.1016/0008-8846(73)90085-9 (URL http://www.sciencedirect.com/science/article/pii/0008884673900859).

[58] S. Brunauer, Surfaces of solids, Pure Appl. Chem. 10 (4) (1965) 293–308, http://dx.doi.org/10.1351/pac196510040293 (URL http://www.iupac.org/publications/pac/10/4/0293/).

[59] Z.P. Bazant, J. Planas, 084938284X, 978–0849382840, Fracture and Size Effect in Concrete and Other Quasibrittle Materials (New Directions in Civil Engineering), 1st edition CRC Press, 1997.
[60] H.M. Jennings, Refinements to colloid model of C–S–H in cement: CM-II, Cem. Concr. Res. 38 (3) (2008) 275–289, http://dx.doi.org/10.1016/j.cemconres.2007.10.006 (URL http://www.sciencedirect.com/science/article/pii/S0008884607002761).
[61] Z. Bažant, Size effect in blunt fracture: concrete, rock, metal, J. Eng. Mech. 110 (4) (1984) 518–535, http://dx.doi.org/10.1061/(ASCE)0733-9399(1984)110:4(518) (URL http://ascelibrary.org/doi/abs/10.1061/).
[62] F. Celarie, S. Prades, D. Bonamy, L. Ferrero, E. Bouchaud, C. Guillot, C. Marlière, Glass breaks like metal, but at the nanometer scale, Phys. Rev. Lett. 90 (7) (2003) 075504, http://dx.doi.org/10.1103/PhysRevLett.90.075504 (URL http://link.aps.org/doi/10.1103/PhysRevLett.90.075504).
[63] C.G. Hoover, Z.P. Bažant, Comprehensive concrete fracture tests: size effects of types 1 & 2, crack length effect and postpeak, Eng. Fract. Mech. 110 (2013) 281–289, http://dx.doi.org/10.1016/j.engfracmech.2013.08.008 (URL http://www.sciencedirect.com/science/article/pii/S0013794413002749).
[64] C.G. Hoover, Z.P. Bažant, Cohesive crack, size effect, crack band and work-of-fracture models compared to comprehensive concrete fracture tests, Int. J. Fract. (2014) 1–11, http://dx.doi.org/10.1007/s10704-013-9926-0 (URL http://link.springer.com/article/10.1007/s10704-013-9926-0).
[65] C.G. Hoover, Z.P. Bažant, J. Vorel, R. Wendner, M.H. Hubler, Comprehensive concrete fracture tests: description and results, Eng. Fract. Mech. 114 (2013) 92–103, http://dx.doi.org/10.1016/j.engfracmech.2013.08.007 (URL http://www.sciencedirect.com/science/article/pii/S0013794413002737).
[66] Z.P. Bazant, Scaling of Structural Strength, Elsevier edition Butterworth-Heinemann, 2005.